Appl Microbiol Biotechnol (2006) 72: 263–278
DOI 10.1007/s00253-005-0247-8

J. L. van Roon · M. M. H. D. Arntz · A. I. Kallenberg · M. A. Paasman · J. Tramper · C. G. P. H. Schroën · H. H. Beeftink

A multicomponent reaction–diffusion model of a heterogeneously distributed immobilized enzyme

Received: 1 July 2005 / Revised: 29 October 2005 / Accepted: 5 November 2005 / Published online: 6 January 2006

Abstract A physical model was derived for the synthesis of the antibiotic cephalexin with an industrial immobilized penicillin G acylase, called Assemblase. In reactions catalyzed by Assemblase, less product and more by-product are formed in comparison with a free-enzyme catalyzed reaction. The model incorporates reaction with a heterogeneous enzyme distribution, electrostatically coupled transport, and pH-dependent dissociation behavior of reactants and is used to obtain insight in the complex interplay between these individual processes leading to the suboptimal conversion. The model was successfully validated with synthesis experiments for conditions ranging from heavily diffusion limited to hardly diffusion limited, including substrate concentrations from 50 to 600 mM, temperatures between 273 and 303 K, and pH values between 6 and 9. During the conversion of the substrates into cephalexin, severe pH gradients inside the biocatalytic particle, which were previously measured by others, were predicted. Physical insight in such intraparticle process dynamics may give important clues for future biocatalyst design. The modular construction of the model may also facilitate its use for other bioconversions with other biocatalysts.

Introduction

Because biocatalyst costs are usually relatively important in bioconversions, they are often immobilized to enhance their stability and facilitate their reuse or continuous utilization (Tramper et al. 2001). During a biocatalytic conversion with an immobilized enzyme, the net fluxes of substrates and products in and out the biocatalytic particles, in case of a diffusion-controlled transport, are driven by radial concentration gradients of the reactants. The local steepness of these gradients is determined by a balance between conversion rates and transport rates, therefore depending on particle size, enzyme loading, particle porosity, and intraparticle reactant diffusivity. As a result of intraparticle reactant gradients, the immobilized biocatalyst operates at concentrations that differ from external bulk liquid concentrations, which is often reflected in the effectiveness factor of a biocatalytic particle. However, if multiple reactions are involved, differences in reactant diffusivities may additionally cause a shift in the relative reaction rates, promoting or inhibiting wanted and unwanted reactions. An example of a system in which such phenomena are relevant is the Assemblase-catalyzed cephalexin synthesis (Fig. 1).

Assemblase is an in-house biocatalytic particle of DSM Anti-Infectives (Delft, The Netherlands). It contains immobilized penicillin G acylase that catalyzes, among others, the synthesis of the widely used semisynthetic antibiotic cephalexin. A single batch was donated for the present research, and in all instances where the trademark Assemblase is used, this refers to this particular preparation. The cephalexin (CEX) synthesis reaction catalyzed by Assemblase is kinetically controlled, and the reaction is stopped before thermodynamic equilibrium is reached (Schroën et al. 2001), implying the need for a transient description of the reaction progress. CEX synthesis (Fig. 1) involves a 2-step coupling reaction of an amide-activated phenylglycine (PGA) with 7-amino deacetoxy cephalosporinic acid (7-ADCA), via an enzyme-phenylglycine complex. The enzyme also catalyzes two unwanted side reactions. In the first, PGA is hydrolyzed to the inactive by-product D-(−)-phenylglycine (PG). In the second, CEX is hydrolyzed to yield 7-ADCA and PG. Schroën et al. (2002) showed that transport of multiple reactants limited each reaction differently. Overall, it was shown that diffusion

J. L. van Roon (✉) · M. M. H. D. Arntz · J. Tramper · C. G. P. H. Schroën · H. H. Beeftink
Department of Agrotechnology and Food Science,
Food and Bioprocess Engineering Group,
Wageningen University,
P.O. Box 8129, 6700 EV, Wageningen, Netherlands
e-mail: Jeroen.vanRoon@wur.nl
Tel.: +31-317-484708
Fax: +31-317-482237

A. I. Kallenberg · M. A. Paasman
DSM Anti-Infectives B.V.,
P.O. Box 425, 2600 AK, Delft, Netherlands

limitations in Assemblase cause a reduced cephalexin production rate, a reduced yield on substrate, and an increased formation rate of the unwanted by-product PG in comparison with the free enzyme (Schroën et al. 2002). On top of that, the intraparticle enzyme distribution of Assemblase was found to be heterogeneous (Van Roon et al. 2005a), which is expected to have a severe impact on the macroscopic particle behavior as well.

To describe the behavior of the immobilized biocatalyst, various types of models can be used, which may differ in the amount of detail in which physical and chemical processes are accounted for. Schroën et al. (2002) adapted their own model for free penicillin G acylase kinetics to one for Assemblase by lumping all relevant phenomena of the biocatalytic particle into a new set of fitted pseudokinetic constants. Although their description of macroscopically observed kinetics was quite good, the fitted constants are only valid for the reaction conditions and biocatalyst preparations they were derived for. Such lumped models are not suited for rational design of new biocatalytic particles, as the constants relate to multiple effects simultaneously. It is obvious that for this specific purpose, a physical model, which accounts for reaction kinetics and mass transfer separately, should be used. This requires extensive knowledge on all the relevant processes in the system, which may be time consuming, but is indispensable for rational biocatalyst design.

In this paper, we present a model that is based on enzyme kinetics of free enzyme, mass transfer in the biocatalytic particle, and the enzyme gradient that is present inside the biocatalytic particle. All these aspects were studied and the obtained constants are truly independent of each other, unlike the constants in the lumped model.

Intrinsic kinetic constants k and activation enthalpies (temperature dependence) for CEX synthesis catalyzed by freely suspended penicillin G acylase were adopted from Schroën et al. (2002) and are depicted in Fig. 1. The activity of the free enzyme as a function of the pH was measured and included in our Assemblase model. Effective diffusivities of all substrates and products were measured. The enzyme loading and enzyme distribution in the Assemblase particles were previously measured as a function of the particle radius (Van Roon et al. 2003), which led to the definition of a single, spherical particle with characteristic size, enzyme loading and enzyme distribution.

An important aspect is that all reactants in cephalexin synthesis are weak electrolytes. The charge of the reactants depends on the local pH in the biocatalytic particle. Duggleby et al. (1995) and Svedas et al. (1980) showed that the enzyme has a single amino acid catalytic center and uses one particular charged form of the reactant only. Because the dissociation constants (pKa values) of substrates and products are different, local enzymatic conversion will result in a change in pH. The fact that all reactants are weak electrolytes also implies that their transport is coupled electrostatically. Electrostatic interactions were modeled by using the Nernst–Planck flux equation for each charged component (e.g., Perry and Green 1997). Based on local transport of reactants and local enzyme kinetics, the pH gradients were predicted, which were used to calculate the local average charge of each weak electrolyte and the local enzyme activity.

The phenomena mentioned above, i.e., enzyme kinetics, mass transfer, enzyme distribution, and dissociation effects, were accounted for to obtain a model for the dynamic progress of cephalexin synthesis. In the literature, several published papers focus on some of these phenomena. Intrinsic kinetic parameters have been published by Schroën et al. (2002). In addition, papers on all sorts of reaction–diffusion systems can be found. Van der Wielen (1994) modeled the enzymatic deacylation of penicillin G into phenylacetic acid and 6-aminopenicillanic acid taking coupled electrostatic transport of ionic species into account. The influence of heterogeneous enzyme distributions in systems with nonionic reactants and with relatively simple enzyme kinetics (zeroth order, first order, and Michaelis–Menten) was investigated by Do and Hossain (1986) and Hossain and Do (1989), who fitted some extreme intraparticle enzyme distributions to macroscopic data sets.

To the best of our knowledge, all these aspects are now brought together for the first time for one immobilized biocatalytic system. The prediction of the macroscopic

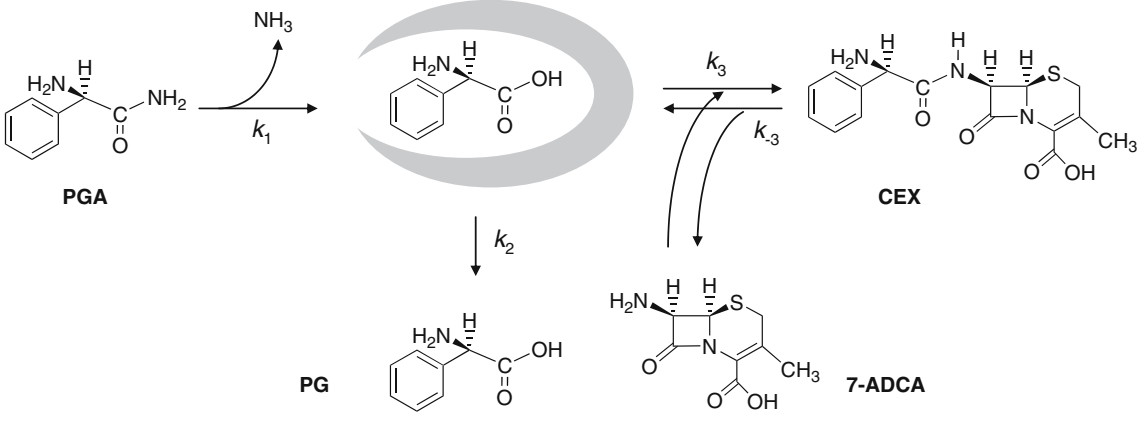

Fig. 1 Production of cephalexin (CEX) from D-(−)-phenylglycine (PGA) and 7-amino deacetoxy cephalosporinic acid (7-ADCA) via an enzyme phenylglycine complex (*gray*). Besides the CEX synthesis reaction, the enzyme also catalyzes two unwanted side-reactions: PGA and CEX hydrolysis, respectively

course of the reaction was successfully validated against experimental data for various temperatures, external pH values, enzyme loadings, and substrate concentrations. The model was used to evaluate the effects of various modifications to the biocatalytic particles, such as alternative enzyme loadings and distributions. In this light, the potential use of the model for further biocatalyst improvement is discussed.

Materials and methods

Definition of a model system

As stated previously, the model is based on enzyme kinetics, enzyme distribution inside the biocatalytic particle, and mass transfer of all reactants. Because we are dealing with charged components, dissociation has to be taken into account also. For cephalexin synthesis with Assemblase, the terms for mass transfer, association/dissociation, and enzyme kinetic rates are stated in Eq. (1):

$$\left(\frac{\mathrm{d}c_{\mathrm{CEX}^-}}{\mathrm{d}t}\right)_{\mathrm{in}} = M_{\mathrm{CEX}^-} + r_{\mathrm{CEX}} + R_{\mathrm{CEX}^-} \quad (1)$$

The net change in the local intraparticle concentration of (negatively charged) cephalexin (c_{CEX^-}, mol·m^{-3}) in time t (s) involves a mass transport rate of CEX^- (M_{CEX^-}, mol·m^{-3}·s^{-1}), the production rate of CEX^- by dissociation (r_{CEX}, mol·m^{-3}·s^{-1}), and the enzyme-catalyzed production rates of CEX^- (R_{CEX^-}, mol m^{-3} s^{-1}). To understand the mechanisms resulting in Assemblase behavior (in comparison with the reaction catalyzed by the free enzyme), each of these three contributions is discussed below. Before this, some basic particle characteristics are defined.

Particle

Geometry and particle size

It was shown previously that Assemblase particles are polydisperse (Van Roon et al. 2003) and, to some extent, polymorph (Van Roon et al. 2005b). A formal treatment of mass transfer processes in such particles would involve an exact three-dimensional analysis of each particle and its contribution to the total volume (or mass) of biocatalytic particles, which is extremely laborious. Instead, spherical particle geometry was assumed; scanning electron microscopic (Van Roon et al. 2005b) micrographs of supercritically dried Assemblase particles indicate that this assumption is not too far off. From the particle size distribution (Van Roon et al. 2003), a characteristic particle was defined as the particle at the 50% point of the cumulative volume distribution (205-μm radius). Assemblase was modeled as if it exclusively consisted of spherical particles of this radius.

Enzyme loading and enzyme distribution

The enzyme loading and distribution were previously measured for multiple particle sizes (Van Roon et al. 2005a). It was shown that all size-dependent intraparticle enzyme distributions within Assemblase had the mathematical shape of in-stationary enzyme penetration profiles and could be described with a Fourier number as a function of the particle radius. From this, the actual enzyme gradient for the characteristic 205-μm particle was obtained by interpolation. This relative distribution was combined with the measured active enzyme loading of 0.95 μmol/g dry weight (DW) and a solidity (g dry weight per g wet weight) of 0.13 (Van Roon et al. 2003) to obtain the quantitative active enzyme distribution of the characteristic particle (Fig. 2). The amount of Assemblase used per experiment varied between 0.5 and 2% of wet particles on mass basis. Typically, 1% of wet biocatalytic particles on total weight was used. The actual particle weight used was inputted for the model prediction. The enzyme gradient in Fig. 2 corresponds with a Fourier value of 8.27×10^{-2} (−) with a standard deviation of 0.97×10^{-2} (−), and it is in very good agreement with the gradient that was measured for an actual particle of 210-μm radius (Van Roon et al. 2003).

Kinetics

Intrinsic enzyme kinetics

Schroën et al. 2002 derived kinetic equations for product and by-product formation using the King–Altman approach. Duggleby et al. (1995) and Svedas et al. (1980) found that the enzyme only binds PGA and 7-ADCA if the amino group is neutral (the carboxylic acid group can be

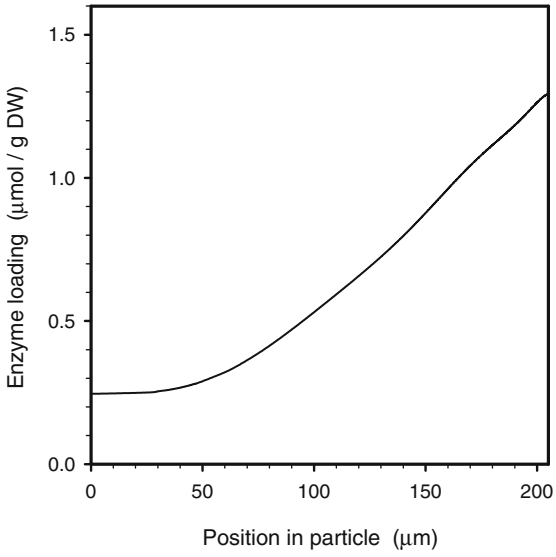

Fig. 2 Characteristic intraparticle enzyme profile for the characteristic Assemblase particle. The enzyme profile corresponds with a Fourier value 0.082 with an average enzyme loading of 0.95 μmol/g DW

either negatively charged or neutral). For this, the rates are expressed in terms of concentrations of the active form:

$$\begin{aligned} R_{\mathrm{PGA}^0} &= \left(-k_1 k_2' c_{\mathrm{PGA}^0} - k_1 k_3 c_{\mathrm{PGA}^0} c_{7-\mathrm{ADCA}^-}\right) \cdot E_0/\Sigma \\ R_{\mathrm{CEX}^-} &= \left(k_1 k_3 c_{7-\mathrm{ADCA}^-} c_{\mathrm{PGA}^0} - k_2' k_{-3} c_{\mathrm{CEX}^-}\right) \cdot E_0/\Sigma \\ R_{\mathrm{PG}^0} &= \left(k_1 k_2' c_{\mathrm{PGA}^0} + k_2' k_{-3} c_{\mathrm{CEX}^-}\right) \cdot E_0/\Sigma \\ \Sigma &= k_1 c_{\mathrm{PGA}^0} + k_2' + k_3 c_{7-\mathrm{ADCA}^-} + k_{-3} c_{\mathrm{CEX}^-} \end{aligned} \quad (2)$$

with R_{PGA^0}, R_{CEX^-} and R_{PG^0} are the net rates of formation of neutral PGA^0, negatively charged CEX^-, and neutral PG^0 ($\mathrm{mol \cdot m^{-3} \cdot s^{-1}}$), respectively, and E_0 is the initial enzyme concentration (g enzyme per g total). Values for the intrinsic kinetic constants k for CEX synthesis catalyzed by freely suspended penicillin G acylase were adopted from Schroën et al. (2002) (Fig. 1). The enzyme can only convert substrates with a neutral amino group. As reactants of cephalexin are weak electrolytes, the fraction of a particular reactant present in its active form depends on the local pH via its dissociation constant K_a ($\mathrm{mol \cdot m^{-3}}$). As an example, Eq. (3) shows the dissociation of CEX^0 into CEX^-:

$$\mathrm{CEX}^0 \underset{r_{-\mathrm{CEX}}}{\overset{r_{\mathrm{CEX}}}{\rightleftharpoons}} \mathrm{CEX}^- + \mathrm{H}^+ \quad (3)$$

The concentrations of CEX^0 and CEX^- are interrelated by their equilibrium constant K_{CEX} ($\mathrm{mol \cdot m^{-3}}$):

$$K_{\mathrm{CEX}} = \left.\frac{c_{\mathrm{CEX}^-} c_{\mathrm{H}^+}}{c_{\mathrm{CEX}^0}}\right|_{\mathrm{eq}} \quad (4)$$

Obviously, for all other reactants, similar equations hold and should be taken into account in the model (see also Table 1). Other components present are Na^+, which is the counter ion, and $\mathrm{NH_3}$, which is liberated during the binding step of PGA with the enzyme.

Temperature and pH dependency of the enzyme

For the temperature dependency of all reaction rate constants, the Arrhenius equation was used (Van't Riet and Tramper 1991), because the activation enthalpies (reaction enthalpies) were assumed to be constant. Data for free enzyme were taken from Schroën et al. (2002):

$$k_{k,T} = k_{k,T_{\mathrm{ref}}} e^{\frac{-\Delta_{H_k}}{R}\left(\frac{1}{T}-\frac{1}{T_{\mathrm{ref}}}\right)} \quad (5)$$

with $k_{k,\,T}$ the reaction rate constant at temperature T, $k_{k,T_{\mathrm{ref}}}$ the reaction rate constant at reference temperature (T_{ref}=293 K), and ΔH_k the reaction enthalpy ($\mathrm{kJ \cdot mol^{-1}}$).

The enzyme activity as a function of pH was investigated with free suspended penicillin G acylase. The relative activity was assessed between pH values of 6.0 and 9.0 (at 0.5 unit intervals) in cephalexin synthesis experiments from 100 mM PGA to 100 mM 7-ADCA at 293 K containing 0.59 μM penicillin G acylase. Between pH 6.0 and 8.0, the relative activity was constant (data not shown). At pH 9.0, 80% residual activity (compared to pH 8.0) remained; the enzyme activity in the model was adjusted accordingly.

Mass transfer

The diffusivities of the reactants were measured at 293 K. At other temperatures, the diffusivities were corrected by application of the generally applied Stokes–Einstein relation (e.g., Bird et al. 1960a,b). Based on the measured diffusivities at 293 K, this equation was first used to estimate the hydrodynamic reactant radius. Subsequently, combination with tabulated values of the dynamic viscosity of water (e.g., Weast and Astla 1980) as a function of temperature led to an estimate of the diffusivity at other temperatures.

Location of mass transfer resistance

It was determined whether there were large differences in the internal and external mass transfer resistance. If so, the model only needs to describe the processes in the most limited region. The Biot number *Bi* describes the dimensionless ratio of the internal and external mass transfer resistances for a component k, and is defined as:

$$Bi_k = \frac{k_{l,k} L}{D_{\mathrm{eff},k}} = Sh_k \frac{D_{l,k}}{D_{\mathrm{eff},k}} \frac{L}{d_p} \quad (6)$$

Table 1 Dissociation constants for weak electrolytes involved in CEX synthesis and effective intraparticle enzyme diffusivities of reactants at 298 K

Component	$\mathrm{PGA^+/PGA^0}$	NH_4^+/NH_3	$\mathrm{7\text{-}ADCA^0/7\text{-}ADCA^-}$	$\mathrm{CEX^0/CEX^-}$	$\mathrm{PG^0/PG^-}$	$\mathrm{H^+}$	$\mathrm{OH^-}$	$\mathrm{Na^+}$	$\mathrm{Cl^-}$
p*K*a $\mathrm{RNH_2}$ (-)	7.2	9.4	4.9	7.6	9.0	–	–	–	–
p*K*a RCOOH (-)	<1.0	–	3.0	2.6	2.0	–	–	–	–
D_{eff} (10^{-10} $\mathrm{m^2/s}$)	4.3[a]	15[b]	3.0[a]	2.5[a]	4.7[a]	70[b]	40[b]	10[b]	15[b]

[a]Measured in this study (see also Fig. 2)
[b]Estimated at 75% of the free-water diffusion coefficient at infinite dilution (Cussler, 2002)

with $k_{l,\,k}$ the mass transfer coefficient of component k in the stagnant layer surrounding the particles, L a characteristic length (here the volume to surface ratio of the particle), $D_{\mathrm{eff},\,k}$ and $D_{l,\,k}$ the intraparticle effective and external free-solution diffusivities of component k ($m^2 \cdot s^{-1}$), respectively, d_p the particle diameter (m), and Sh the Sherwood number for mass transfer, which is the ratio of total mass transfer and diffusive mass transfer in the continuous phase surrounding the particles. The value of the Sherwood number Sh was estimated with the empirical relation by Brian and Hales, Eq. (7) (Van't Riet and Tramper 1991):

$$Sh_k = 2 + 0.57\sqrt{Re}\left(\frac{\eta_l}{\rho_l D_{l,k}}\right)^{0.33} \tag{7}$$

with Re the Reynolds number for the particle (calculated to be 3 from the Galileo number), ρ_l the water density (1,000 $kg \cdot m^{-3}$), and η_l the dynamic viscosity of the continuous phase (1×10^{-3} Pa·s). Depending on the diffusing compound, a value of approximately 20 was calculated for Sh, resulting in Bi values of 5–10. On this basis, external mass transfer resistance was neglected in the model.

Because the resistance for mass transfer is situated in the particle interior, the diffusivities of the reactants inside the particles were measured likewise. This was done with a portion of the same preparation of Assemblase particles that was not activated with enzyme. A known amount of these wet sieved (Van Roon et al. 2003) particles was incubated overnight at 277 K and pH 8.0 in a solution in which a known amount of reactant was dissolved. Then the equilibrium concentration of the reactant in the continuous phase was analyzed by high-performance liquid chromatography (Van Roon et al. 2003) to check for partitioning. A portion of these particles was transferred into a known amount of water that was vigorously stirred. Particle-free samples were taken immediately (by use of filters), and the concentration was measured with HPLC. From this, the diffusivity was estimated by fitting a standard parabolic differential equation for Fickian diffusion (e.g., Bird et al. 1960a,b) out of a known mass of spheres of 205-μm radius. As an example, the measured concentrations and fitted concentration profile of PG is given in Fig. 3. The effective PG diffusivity that fitted the data best was 4.7×10^{-10} $m^2 \cdot s^{-1}$. The diffusivities of the other reactants were fitted similarly and their values are given in Table 1.

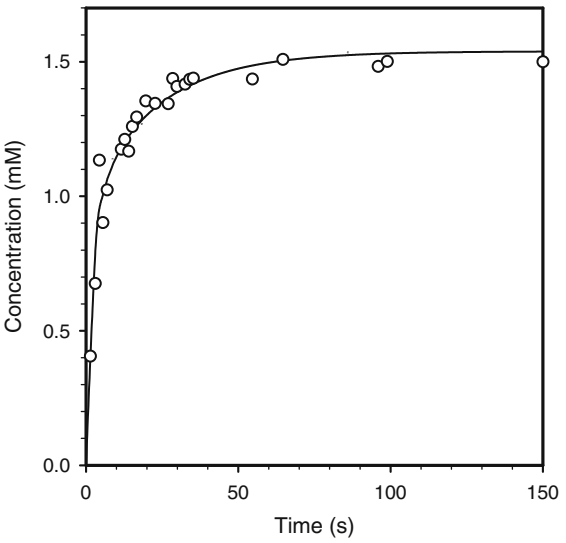

Fig. 3 Measured PG concentration in the continuous phase in time (*points*) and the fitted concentration profile for an effective intraparticle PG diffusivity of 4.7×10^{-10} $m^2 \cdot s^{-1}$ at an initial intraparticle PG concentration of 19 mmol/kg WW (13% solidity) and 7% w/w particle hold-up

Mass transport rate and flux equations

Because the particles are assumed to be spherical, radial symmetry can be assumed and the mass balances can be solved one-dimensionally (along the radial axis). The rate equation for diffusion of species k into a spherical particle along the space coordinate x (m):

$$M_k = \frac{1}{x^2}\frac{\mathrm{d}}{\mathrm{d}x}\left(x^2 J_k\right) \tag{8}$$

with M_k the rate of the concentration change of component k ($mol \cdot m^{-3} \cdot s^{-1}$) and J_k the mass flux of component k ($mol \cdot m^{-3} \cdot s^{-1}$). The Nernst–Planck equation was used for all components, which describes the flux of a charged component as a function of a concentration gradient and a potential gradient:

$$J_k = D_{k,\mathrm{eff}}\left(\frac{\mathrm{d}c_k}{\mathrm{d}x} + z_k c_k \frac{F}{RT}\frac{\mathrm{d}\Phi}{\mathrm{d}x}\right) \tag{9}$$

with J_k as the flux of component k ($mol \cdot m^{-3} \cdot s^{-1}$), z_k is the charge of component k (−), F the Farraday constant ($C \cdot mol^{-1}$), R the gas constant ($J \cdot mol^{-1} \cdot K^{-1}$), T the temperature (K), and Φ the electrical potential (V). For uncharged components (z_k=0), Eq. (9) reduces to the Fickian flux equation. The potential gradient was eliminated from the system by assuming a zero net electrical current:

$$\sum_{k=1}^{N} z_k J_k = 0 \tag{10}$$

where N equals the total number of components (−). From Eqs. (9) and (10), it can be derived that:

$$\frac{\mathrm{d}\Phi}{\mathrm{d}x} = -\frac{RT}{F}\frac{\sum_{k=1}^{N} z_k D_{k,\mathrm{eff}}\,\mathrm{d}c_k/\mathrm{d}x}{\sum_{k=1}^{N} z_k^2 D_{k,\mathrm{eff}} c_k} \tag{11}$$

which can be substituted in Eq. (9):

$$J_k = D_{k,\mathrm{eff}}\left(\frac{dc_k}{\mathrm{d}x} - z_k c_k \frac{\sum_{k=1}^{N} z_k D_{k,\mathrm{eff}}\,\mathrm{d}c_k/\mathrm{d}x}{\sum_{k=1}^{N} z_k^2 D_{k,\mathrm{eff}} c_k}\right) \tag{12}$$

Internal mass balances

Now that all parts of Eq. (1) have been discussed in more detail, we will focus on the association and dissociation reactions. The (de-)protonation rate (r_{CEX}) from Eq. (1) is extremely fast in comparison with the enzymatic reaction rates (R_{CEX} in Eq. 1). The different time constants for the two processes dramatically increase the stiffness of the system of mass balances and may result in long calculation times or even in numerical instabilities. Therefore, fast (de-)protonation rates were eliminated taking convenient linear combinations of the differential mass balances and regarding the (de-)protonation rates to be infinitely fast in comparison with the enzymatic conversion rates, analogous to the procedure by Van der Wielen (1994). For the example given in Eq. (1), a suitable linear combination is:

$$\begin{aligned}\left(\mathrm{d}c_{\mathrm{CEX}^-}/\mathrm{d}t\right)_{\mathrm{in}} &= M_{\mathrm{CEX}^-} + r_{\mathrm{CEX}} + R_{\mathrm{CEX}^-}\\ \left(\mathrm{d}c_{\mathrm{CEX}^0}/\mathrm{d}t\right)_{\mathrm{in}} &= M_{\mathrm{CEX}^0} - r_{\mathrm{CEX}}\end{aligned} \tag{13}$$

The equation illustrates that the neutral form of cephalexin cannot be formed by the enzyme. By adding these two equations, the fast association rates cancel out. With the assumption of infinitely fast deprotonation reactions, the concentration of neutral cephalexin is instantly dictated by the association constant of cephalexin, and the concentrations of negatively charged cephalexin and protons Eq. (4), and the rate equation becomes:

$$\left(\frac{\mathrm{d}c_{\mathrm{CEX}^-}}{\mathrm{d}t}\right)_{\mathrm{in}} = \frac{M_{\mathrm{CEX}^-} + M_{\mathrm{CEX}^0} + R_{\mathrm{CEX}} - \frac{c_{\mathrm{CEX}^-}}{K_{\mathrm{CEX}}}\frac{\mathrm{d}c_{\mathrm{H}^+}}{\mathrm{d}t}}{1 + c_{\mathrm{H}^+}/K_{\mathrm{CEX}}} \tag{14}$$

Equation (14) shows that the concentration change of CEX^- in time is not only affected by its enzymatic conversion and the its flux, but also by the flux of its uncharged counterpart CEX^0. Furthermore, it is also directly affected by the local pH and the pH gradient. The example given above also applies for other weak electrolytes. The p*K*a values of all the components in the model are summarized in Table 1.

In all association/dissociation reactions, protons are bound or released. For all weak electrolytes, the internal pH gradient is influenced by all these equilibriums and vice versa. An exception to this is 7-ADCA, of which the p*K*a values are so low that its charge is almost exclusively negative in the pH regions where the reactions take place. Therefore, 7-ADCA is conveniently regarded as a strong electrolyte with a negative charge. Because protons are released or used in the deprotonation and protonation reactions of every weak electrolyte, respectively, the mass balance becomes complex; it is therefore given in the "Appendix."

External mass balances

The mass balances over the continuous phase surrounding the particles were derived analogous to the internal mass balances. The two differences are the obvious absence of enzyme in the continuous phase of the reactor, and the time dependent volume increase of the water phase, which is a result of titration with hydrochloric acid during the conversion to keep the external pH constant. In Eqs. (15) and (16), the external mass balances for PGA^0 and PGA^+ are given:

$$\left(\frac{\mathrm{d}c_{\mathrm{PGA}^0}}{\mathrm{d}t}\right)_{\mathrm{ex}} = M_{\mathrm{PGA}^0} + r_{\mathrm{PGA}} - \frac{c_{\mathrm{PGA}^0}}{V_{\mathrm{c}}}\frac{\mathrm{d}V_{\mathrm{c}}}{\mathrm{d}t} \tag{15}$$

$$\left(\frac{\mathrm{d}c_{\mathrm{PGA}^+}}{\mathrm{d}t}\right)_{\mathrm{ex}} = \frac{\mathrm{d}c_{\mathrm{PGA}^0}}{\mathrm{d}t} = M_{\mathrm{PGA}^+} - r_{\mathrm{PGA}} - \frac{c_{\mathrm{PGA}^+}}{V_{\mathrm{c}}}\frac{\mathrm{d}V_{\mathrm{c}}}{\mathrm{d}t} \tag{16}$$

with V_c as the volume of the continuous (water) phase (m^3). Linear combination of these equations to eliminate the fast association/dissociation rates (analogous to Eq. 14) results in:

$$\left(\frac{\mathrm{d}c_{\mathrm{PGA}^0}}{\mathrm{d}t}\right)_{\mathrm{ex}} = \frac{M_{\mathrm{PGA}^0} + M_{\mathrm{PGA}^+} - \frac{c_{\mathrm{PGA}}}{K_{\mathrm{PGA}}}\frac{\mathrm{d}c_{\mathrm{H}^+}}{\mathrm{d}t} - \frac{1}{V_c}\frac{\mathrm{d}V_{\mathrm{c}}}{\mathrm{d}t}\left(c_{\mathrm{PGA}^+} + c_{\mathrm{PGA}^0}\right)}{1 + c_{\mathrm{H}^+}/K_{\mathrm{PGA}}} \tag{17}$$

The titration with hydrochloric acid during the synthesis reaction introduces chloride ions in the system (which will subsequently diffuse into the carrier and were therefore incorporated in the summation term of the internal and external Nernst–Planck flux equations). The chloride ions are considered inert in the model; only electrostatic diffusion of chloride into the particles was accounted for. The volume increase is calculated and used in all external

equations. The two equations are given in the "Appendix" (Eqs. 24 and 25, respectively). For the external chloride mass balance this results in:

$$\left(\frac{\mathrm{d}c_{\mathrm{Cl}^-}}{\mathrm{d}t}\right)_{\mathrm{ex}} = M_{\mathrm{Cl}^-} + \frac{c_{\mathrm{titrant}}}{V_{\mathrm{c}}}\frac{\mathrm{d}V_{\mathrm{c}}}{\mathrm{d}t} - \frac{c_{\mathrm{Cl}^-}}{V_{\mathrm{c}}}\frac{\mathrm{d}V_{\mathrm{c}}}{\mathrm{d}t} \tag{18}$$

Boundary conditions

Because radial symmetry was assumed in all particles, all concentration profiles are symmetric around the particle center. Consequently, all concentration gradients in the particle center are zero, which results in a zero net mass flux through the particle center:

$$(\mathrm{d}c_k/\mathrm{d}x)|_{x=0} = 0 \tag{19}$$

At the particle-bulk interface, no accumulation can take place: the net flux of reactants leaving the continuous phase equals the net flux of reactants entering the combined volumes of the first slabs of the particles. Because external diffusion limitation could be neglected, it follows that:

$$\left(\frac{V_{\mathrm{c}}\mathrm{d}c_{k,\mathrm{c}}}{\mathrm{d}t}\right)_{\mathrm{ex}} = A_{\mathrm{p}}n_{\mathrm{p}}\left|\frac{1}{x^2}\frac{\mathrm{d}}{\mathrm{d}x}\left(x^2J_k\right)\right|_{x=R_{\mathrm{p}}} \tag{20}$$

with J_k given by Eq. (12), V_c the volume of the continuous (water) phase (m^{-3}), A_p the surface area of a single particle (m^2), n_p the number of particles (calculated from mass hold-up and particle density), and $c_{k,\,c}$ the concentration of component k in the continuous (water) phase ($mol \cdot m^{-3}$).

Numerical solving of the mass balances

To numerically solve the parabolic partial differential equations for combined mass transfer and enzyme kinetics, the system of equations was made discrete with respect to the spatial coordinate. A schematic representation of the spatial grid is depicted in Fig. 4. At the left side, the particle center is drawn and the particle perimeter with the surrounding continuous phase is drawn at the right-hand side. An arbitrary transient gradient of a reactant with its highest concentration near the particle surface is drawn in Fig. 4. The gradient is approximated by dividing the particle interior in several volume elements that were each regarded as ideally mixed CSTR's (finite volume method).

The volume of all elements was chosen constant (equivolumetric grid) to save calculation time, without precision loss. Consequently, the model can make do with fewer internal grids in comparison with an equidistant grid. Because the innermost grid covers quite a large distance from the center of the particle, it was refined with equi-

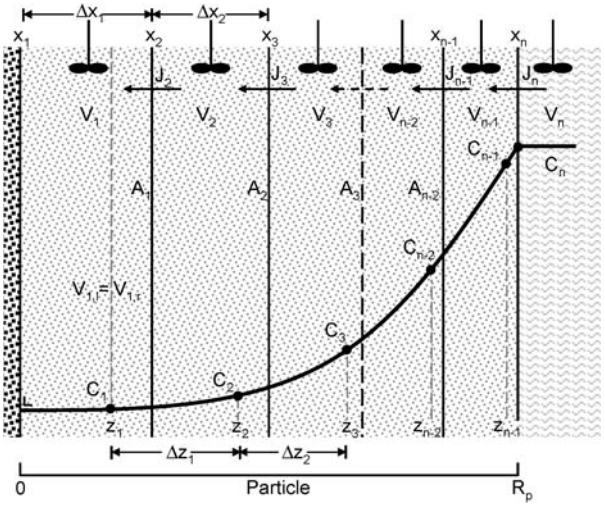

Fig. 4 Grid used for numerical solutions of the differential equations. Equivolumetric volume elements are considered ideal mixers with concentration C_i located at the volumetric center of the grid z_i. Mass fluxes (J) enter and leave at the borders of the volumetric element (x_i) across an area A_i. External diffusion limitation is neglected and the continuous phase is considered ideally mixed

distant subgrids. Figure 4 illustrates that the concentration gradient (slope) of the arbitrary concentration profile of the reactant at the particle center is zero and that the surface concentration (C_n) equals the bulk concentration because external diffusion limitation was neglected.

The average concentration in each element (V_i) is situated at the positions where 50% of the volume of that particular volume element was reached. This concentration is affected by the inflow and outflow of mass (the fluxes are indicated by the arrows) through the boundary areas (A_i) on the two sides of the element and by enzymatic and by association/dissociation reactions, as was explained previously. Two different grids were introduced: one to define the locations of the average concentrations (z-grid) and the other to define the locations of the interfaces through which the fluxes take place (x-grid). Consequently, $\Delta z_1 \neq \Delta x_1$ and the two grid-vectors were used during solving.

A central difference approximation of the second order was used to approximate the concentration derivatives in the mass balances. An example is given for the central difference approximated concentration gradient of arbitrary nonionic reactant k in Fig. 4 at position z_2 in volume element V_2:

$$\begin{aligned}\frac{\mathrm{d}c_{k,2}}{\mathrm{d}z} &\approx \frac{J_{k,3}A_2 - J_{k,2}A_1}{V_2} \\ &= \frac{D_{k,\mathrm{eff}}\left(\frac{c_{k,3}-c_{k,2}}{\Delta z_2}A_2 - \frac{c_{k,2}-c_{k,1}}{\Delta z_1}A_1\right)}{V_2}\end{aligned} \tag{21}$$

The spatially discrete system of the mass balances was solved for all components by use of the ODE-15s solver of Matlab (version 6.5.0). This solver is especially useful to

solve stiff systems to which end it uses a variable order Runge–Kutta algorithm with adaptive time-step to approximate the solution. The concentrations of the conjugated forms of the biocatalytically active weak electrolytes were subsequently calculated by the dissociation constant in each time step. For control purposes, the total charge in the system was calculated for each time step. With the applied precision (32 digit calculation and tolerance settings), the total charge imbalance always remained below 10^{-12} ($mol \cdot m^{-3}$), which is very low, even in comparison with the proton concentrations.

Results

Before validation of our model with data on Assemblase catalyzed reactions, we tested it on enzyme kinetics only. This was done by increasing the diffusion coefficients to very high values. The model should now predict the reaction carried out by free enzyme. The result is shown in Fig. 5a for a reaction previously done for 100 mM of the two substrates at 293 K and pH 8.0 (Schroefn et al. 2002). The model and the measured data are in good agreement therewith indicating that the kinetics was implemented correctly in the model.

External course of the reaction: model validation

Cephalexin (CEX) synthesis experiments at various PGA and 7-ADCA concentrations, pH values, and temperatures were done to check the predictions of the model.

Synthesis with various substrate concentrations

Subsequently, the proper diffusivities were used to check whether the model could predict syntheses reactions catalyzed by Assemblase. Figure 5b shows that for the same reaction conditions used in the free enzyme experiment, the model prediction is in close agreement with the experimental data, and the effect of mass transfer during the synthesis was predicted well. When compared with the free enzyme reaction (Fig. 5a), less CEX and more phenylglycine (PG) is formed during the synthesis with Assemblase. The model could also predict the course of the reaction for other substrate concentrations (Fig. 5c,d). The model was found to predict the experimental data well both at medium-high and very high substrate concentrations indicating that in the current model, mass transfer is also implemented correctly, together with the enzyme gradient. The main difference with the previously published model

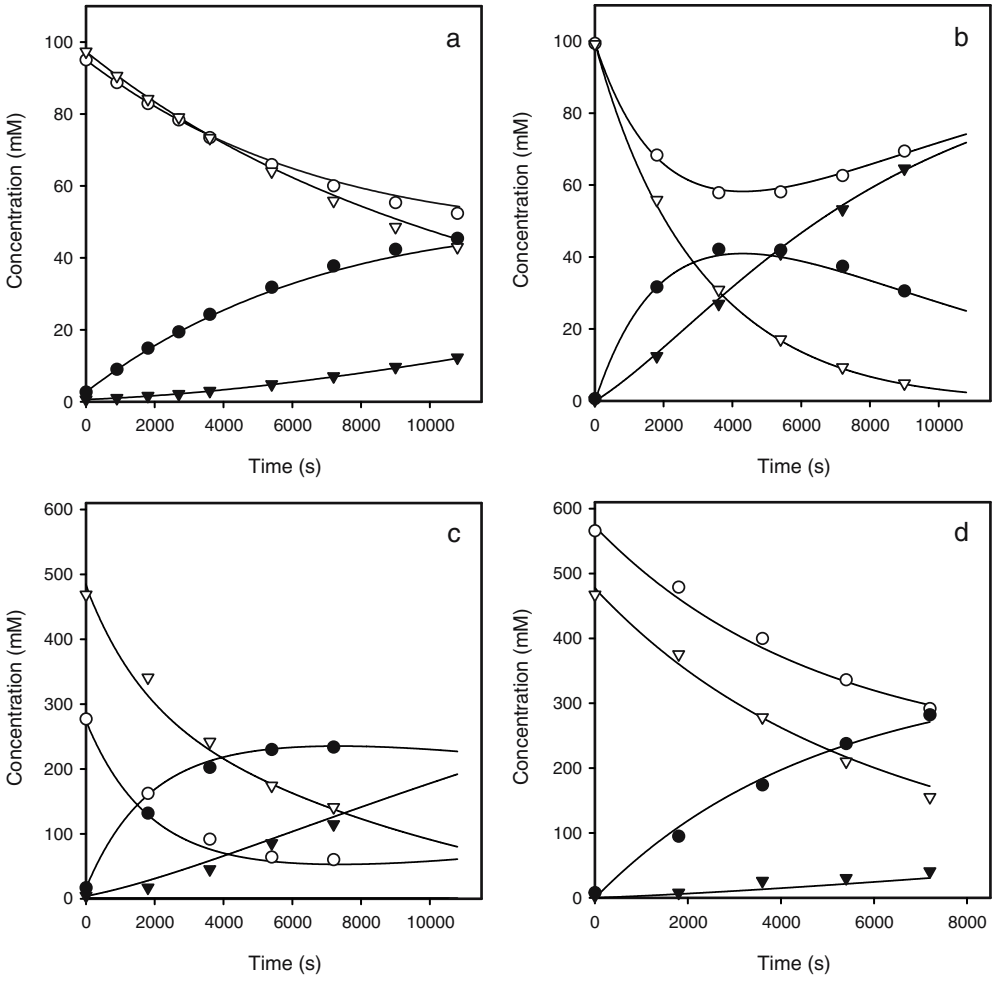

Fig. 5 Predicted (*lines*) and measured (*dots*) total concentrations of PGA, 7-ADCA, CEX and PG during cephalexin synthesis at 293 K and pH 8.0. **a** Model prediction for unrealistically high reactant diffusivities and experimental values for a CEX synthesis with free enzyme from 100 mM of the two substrates. **b** Experimental data and model prediction for CEX synthesis from 100 mM of both PGA and 7-ADCA. **c** Experimental data and model prediction for CEX synthesis from 500 mM PGA and 300 mM 7-ADCA. **d** Experimental data and model prediction for CEX synthesis from 500 mM PGA and 600 mM 7-ADCA. All graphs: *inverted open triangles*, PGA; *inverted full triangles*, PG; *filled circles*, CEX; *open circles*, 7-ADCA

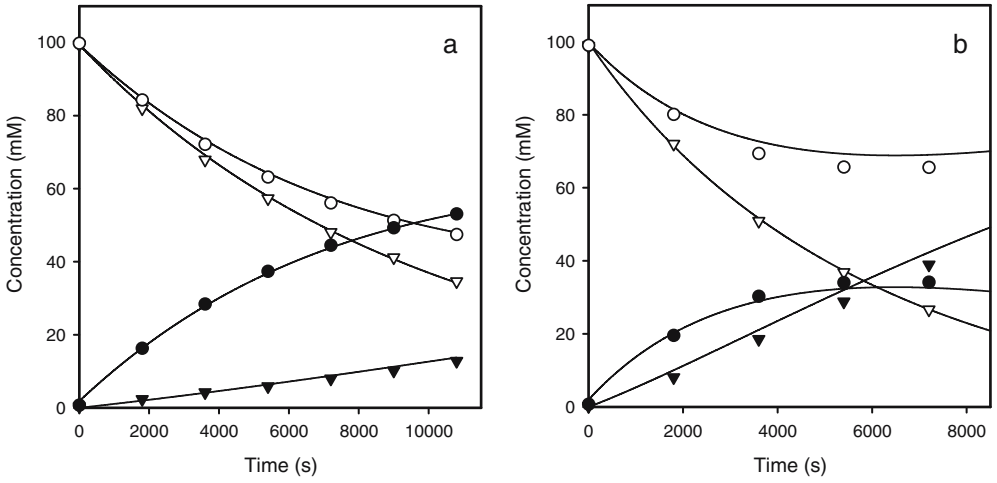

Fig. 6 Predicted (*lines*) and measured (*dots*) total concentrations of PGA, 7-ADCA, CEX, and PG during cephalexin synthesis from 100 mM PGA and 100 mM 7-ADCA, pH 8.0 at 273 K (**a**) and 303 K (**b**), respectively. All graphs: *inverted open triangles*, PGA; *inverted full triangles*, PG; *filled circles*, CEX; *open circles*, 7-ADCA

(Schroën et al. 2002) is that a prediction on the basis of independent physical and chemical phenomena is actually obtained now rather than a description based on pseudo-kinetic parameters that were fitted to the experimental data.

Synthesis experiments at various temperatures

The temperature influences both the rates of reaction and of diffusion. Temperature corrections for the rates of enzymatic reactions were made with the Arrhenius equation, while the temperature dependencies of diffusivities were based on the Stokes–Einstein equation (see "Materials and methods"). To check whether temperature effects were correctly implemented, we tested whether the model predicted reactions carried out between 273 and 303 K correctly.

For the entire temperature range correct predictions were obtained as is illustrated by the result of the two extremes (Fig. 6). With equal amounts of Assemblase, the CEX synthesis at 273 K (Fig. 6a) is approximately 4.3 times slower than at 293 K(Fig. 5b). At 303 K (Fig. 6b), the CEX synthesis is 1.9 times faster than at 293 K for equal enzyme amounts (Fig. 5b). The maximum CEX concentration is highest at lower temperatures: 56 mM at 273 K (Fig. 6a) and 36 mM at 303 K (Fig. 6b). The reason is that the kinetic reaction is more temperature dependent than diffusion: a low-temperature synthesis is therefore less diffusion limited.

Synthesis experiments at various pH values

At the pH that was used until now (8.0), the model predicted the course of the reactions correctly. Now the model is tested at pH values between 6.0 and 9.0. Because the enzyme only uses a specifically charged state of the weakly electrolytic reactants (see "Definition of a model system" section), the ambient pH determines the availability of reactants for reaction and influences the electrostatically coupled transport of electrolytes. Because the pH continuously changes in space and time, prediction of the overall reaction progress is challenging. This can be illustrated by the fact that the course of the reaction at pH<7 could not be described by the lumped model we presented previously (Schroën et al. 2002).

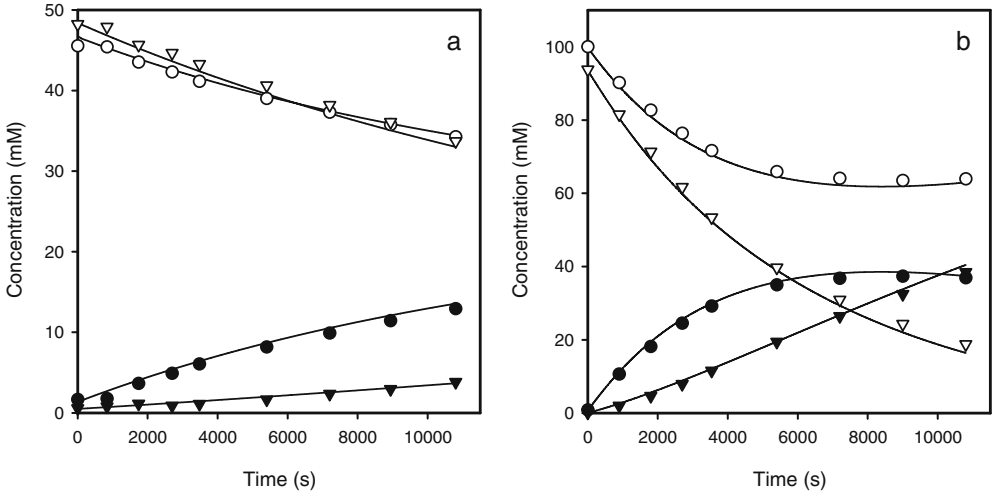

Fig. 7 Predicted (*lines*) and measured (*dots*) total concentrations of PGA, 7-ADCA, CEX, and PG during cephalexin synthesis from PGA and 7-ADCA, 293 K at pH 6.0 (**a**) and 9.0 (**b**), respectively. In the case of pH 6.0, 50 mM of the two substrates was used because of solubility limits. All graphs: *inverted open triangles*, PGA; *inverted full triangles*, PG; *filled circles*, CEX; *open circles*, 7-ADCA

The model predicted the course of the CEX synthesis well for the entire range of pH values. Once again, the predictions for the two extremes are shown (pH 6.0 and 9.0 in Fig. 7a,b, respectively). For pH 9.0, the situation is comparable to pH 8.0 for as far as diffusion limitation is concerned, and these effects are predicted correctly. At pH=6.0, the solubility of the substrates is limited and the experiment was conducted with approximately 50 mM of the two substrates. Figure 7a shows that with the physical model, the prediction of the course of the reaction is good. The fact that reactions are slow at pH 6.0 is not only caused by a reduced enzyme activity at this pH, but is a result of the reduced amounts of reactive PGA and CEX (Schroën et al. 2002). Because the conversion rates are reduced, the particle is less diffusion limited at lower pH. In this case, the course of the reaction is similar to one carried out with free enzyme. As opposed to the pseudokinetic model by Schroën et al. (2002), the present physical model quantitatively predicts these effects ranging from situations that

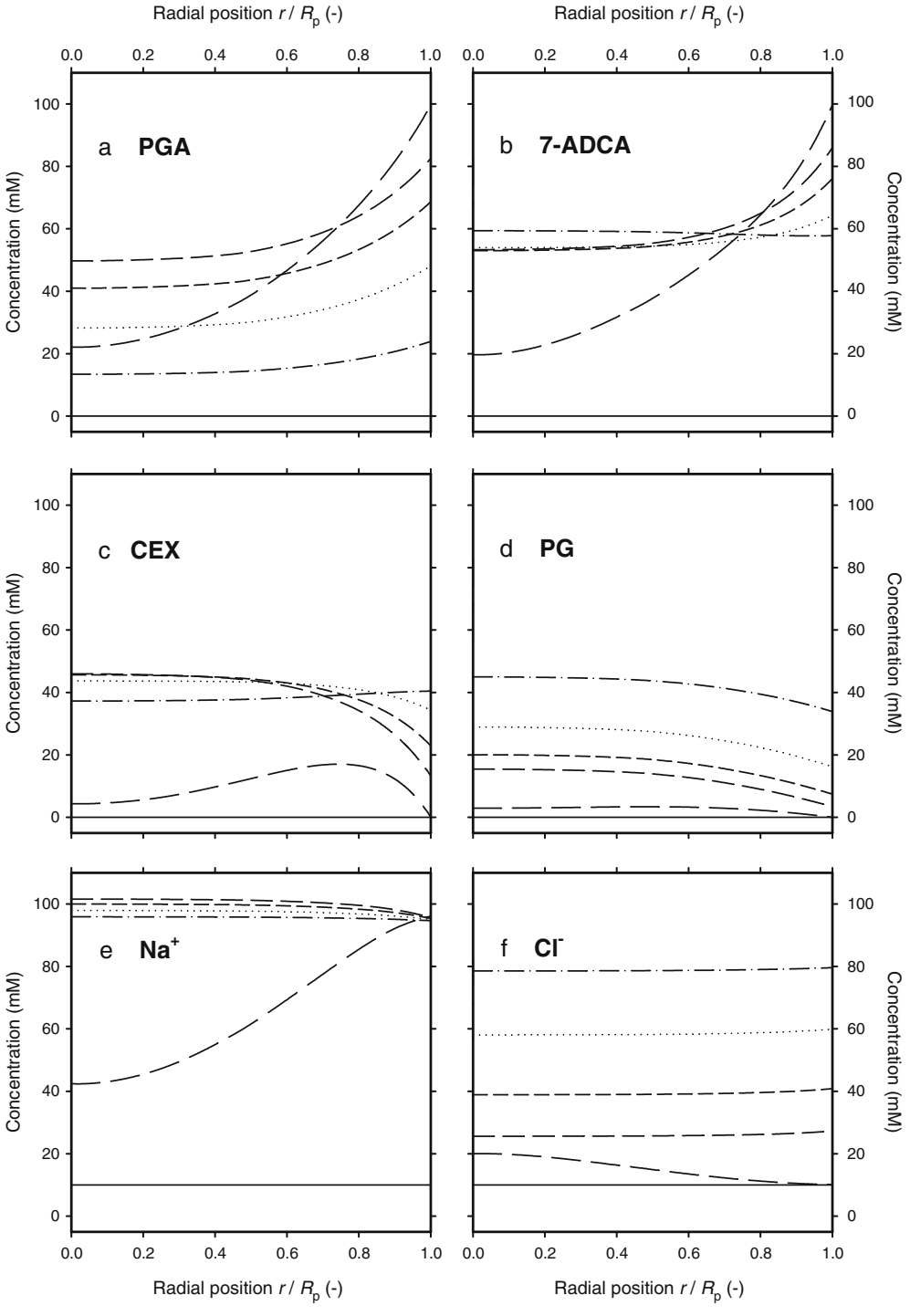

Fig. 8 Model predictions for a 100-mM PGA and 7-ADCA conversion by Assemblase at 293 K. During the experiment, the external pH was kept at 8.0 by 0.5 M HCl titration. **a-f** Prediction of the internal total concentration profiles of PGA, 7-ADCA, CEX, PG, Na^+, and Cl^- after 0 (___); 10 (_ _ _); 1,000 (_ _ _ _); 2,000 (_ _ _ _ _); 4,000 (…….); and 8,000 s (_._._)

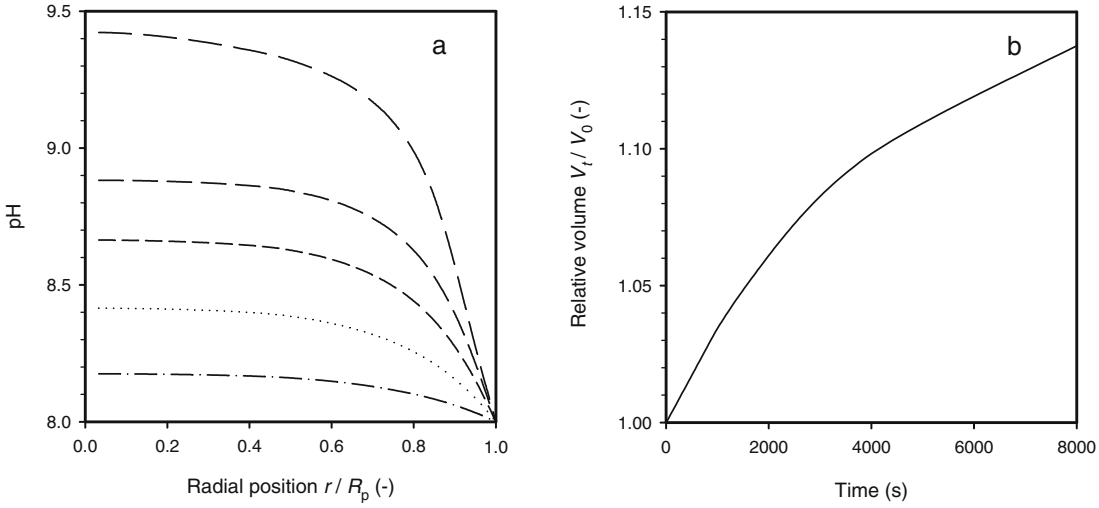

Fig. 9 **a** Predicted internal pH profiles during a 100-mM PGA and 7-ADCA conversion by Assemblase at 293 K after 0 (___); 10 (_ _ _); 1,000 (_ _ _ _); 2,000 (_ _ _ _ _ _); 4,000 (……); and 8,000 s (_._._._). During the experiment, the external pH was kept at 8.0 by 0.5 M HCl titration (see also Fig. 8). **b** Predicted total volume during the conversion. See also Fig. 5b for external concentrations

are heavily diffusion limited to situations that are hardly diffusion limited.

Internal course of the reaction: understanding particle behavior

Until now, the model was successfully validated by comparing the prediction of the external course of the synthesis reaction with the experimental synthesis data. This gives confidence in the validity of the predicted internal gradients of reactants during the conversion (which are very difficult to measure due to their dynamic character). Because insight in intraparticle phenomena can greatly improve our understanding of the biocatalytic system, Fig. 8 gives an overview of dynamic intraparticle gradients of some reactants during the conversion of 100 mM of both PGA and 7-ADCA at pH 8 and 293 K (Fig. 5b).

Immediately upon the addition of the Assemblase particles (start of the reaction), the mobile sodium ion (Fig. 8e) and PGA (Fig. 8a), of which only a part is ionic at pH 8.0, penetrate the particle along their concentration gradient. This transport must be accompanied by influx of negative ions. Anionic transport is partially accounted for by the relatively slow 7-ADCA, which penetrates into the carrier along its concentration and electrical gradient (Fig. 8b), but mainly by the relatively mobile chloride ions (Fig. 8f), for which only an electrical gradient exists (i.e., no concentration gradient). The rapid influx of sodium ions generates an electrical gradient, resulting in transport of negatively charged ions toward the carrier center. Because chloride is the most mobile, it will temporarily diffuse against its concentration gradient (Fig. 8f).

As a result of the substrate fluxes the substrate concentration in the outer regions of the particle rises quickly. Combined with the presence of a relatively high enzyme concentration in the outer region, the cephalexin production rate is relative high there. Because any cephalexin is hardly present in the interior or in the continuous phase, the formed cephalexin temporarily diffuses in both of these directions (Fig. 8c). Because of the volume of the continuous phase, the driving force for transport toward this phase remains high in comparison with the much smaller particle interior (where cephalexin will be generated as well). Internally, the CEX production rate rises as substrates become more available, and the concentration gradient becomes directed toward the bulk phase (Fig 8c). After reaching the maximum CEX concentration in the bulk (as was shown in Fig. 5b, this happens after approximately 4.5×10^3 s), the total CEX hydrolysis rate becomes higher than the CEX production rate, and the concentration gradient reverses again toward the inner regions of the particle (net CEX flux into the particle).

For the by-product of the syntheses, PG, the same happens as with CEX. A temporary accumulation followed by bidirectional diffusion, and subsequently the concentration gradient becomes directed toward the outside of the particle (Fig. 8d). This effect is smaller than for CEX, occurs at a later moment in time, and is situated more internally. Given the temporary cephalexin maximum, this could be expected; CEX will partly be hydrolyzed by the enzyme to form phenylglycine (secondary hydrolysis). Because the equilibrium of the reaction lies completely on the PG side, the total PG production rate remains positive, and the concentration gradient of PG remains directed toward the continuous phase.

Upon binding of PGA to the enzyme, NH_3 is formed. Being the strongest base in the system with a p*K*a value of 9.4, it will take up protons and form NH_4^+, which will cause the local pH to rise. Figure 9a shows that the model predicts an initial increase in pH in the particle center of almost 1.5 pH unit, which quickly diminishes to 0.5–1 pH unit. These values are comparable to values reported by Spieß and Kasche (2001) for CEX synthesis reactions carried out with Assemblase.

Figure 9b shows that the volume of the bulk phase increases because of the external HCl addition for pH control. In the experiment, a moderate titrant concentration of 0.5 M was used to prevent "hot spots" in the reactor. Figure 9b shows that during the synthesis of cephalexin, the rate of HCl addition is continuously decreased. This is in accordance with Fig. 5b that showed that PGA conversion, and therewith the NH_3 production rate, decreases. The effect from this on pH overrules the effect of the increased PG production rate.

Discussion

Figure 8 showed an example of the predicted internal reactant dynamics during CEX synthesis. The internal production rates are lowered as a result of diffusional limitations of multiple reactants. Because the CEX production rate is hampered more than the PG production rate, and the produced CEX remains longer in the carrier, the macroscopic particle behavior of Assemblase is suboptimal for CEX synthesis when compared with free-enzyme catalyzed reactions. To obtain an idea of the sensitivity of the Assemblase system for variations in parameters of the biocatalytic particle, their effect is evaluated in terms of the cephalexin yield on 7-ADCA and the selectivity for product formation. This is expressed as the synthesis/hydrolysis ratio S/H at maximum conversion, i.e., the ratio between the maximum CEX concentration and the accompanying PG concentration.

The sensitivity of the S/H ratio for changes in the values of the kinetic rate constants is discussed elsewhere (Van Roon 2005). The analysis showed that the model predictions were sensitive toward all rate constants; however, the system was particularly sensitive toward the value of the hydrolysis rate constant k_2.

The predicted effects of particle size, enzyme loading, and the distribution of enzyme for some hypothetical situations (model extrapolations) are summarized in Table 2.

Table 2 shows that, with all other parameters identical, smaller particle sizes are favorable for both the product yield and the selectivity for CEX synthesis, as was expected. To keep all other parameters constant, a homogeneous enzyme distribution was used. In a similar way, particles with a lower enzyme loading, i.e., average enzyme concentration over the particle, perform better in terms of product yield and S/H, because particles with low enzyme concentrations are less diffusion limited. For heterogeneously loaded particles, the combination of particle size, enzyme loading, and the enzyme distribution determines the overall yield and selectivity.

With the enzyme in Assemblase predominantly situated in the outer regions of the particle (Van Roon et al. 2005a), the yield and selectivity are better than that of a particle with a homogeneous enzyme distribution and much better than one with an active core (Table 2). This results from an improved supply of 7-ADCA to the enzyme and the reduced secondary hydrolysis of the 'slow' CEX for the case of Assemblase. It is obvious that the yield and selectivity obtained with surface-loaded particles are equal to those of free enzyme, because no diffusional limitations are present.

Industrial application of such hypothetically new biocatalytic particles can be hampered, however, by several aspects. On one hand, there is no production process available to produce the theoretical particles with the properties described above. On the other hand, there are practical limitations to the application of such new particles. For instance, depending on the maximal enzyme binding capacity, it may not be possible to immobilize enough enzyme on the surface of the particles and keep the particle hold-up within practical limits at the same time. The enzyme on surface-loaded particles may also be more sensitive to chemical (hot spots) or mechanical degradation. In addition, very small particles may not be suitable for industrial application.

Table 2 Model prediction of CEX yield on 7-ADCA ($Y_{CEX,7\text{-}ADCA}$) and selectivity for CEX over PG formation (S/H) for particles with different radii R_p, average enzyme loadings E_{avg}, and enzyme distributions

R_p (μm)	E_{avg} (μmol/g DW)	Distribution	$Y_{CEX,7\text{-}ADCA}$ (−)	S/H (−)
5	0.95	Homogeneous	0.48	1.93
50	0.95	Homogeneous	0.47	1.80
250	0.95	Homogeneous	0.37	0.98
500	0.95	Homogeneous	0.31	0.71
205	0.50	Homogeneous	0.42	1.31
205	0.95	Homogeneous	0.39	1.10
205	2.00	Homogeneous	0.36	0.90
205	5.00	Homogeneous	0.32	0.71
205	0.95	Surface loading	0.48	1.93
205	0.95	Assemblase	0.41	1.19
205	0.95	Homogeneous	0.39	1.10
205	0.95	Active core (50 μm)	0.09	0.15

All simulations were done with 100 mM of the two substrates at 293 K and pH 8.0. The S/H was evaluated at the maximal CEX concentration (maximal conversion)

Table 3 Model prediction of CEX yield on 7-ADCA ($Y_{CEX,7\text{-}ADCA}$) and of selectivity for CEX over PG formation (S/H) for diffusivities of 7-ADCA, PGA and CEX for values 5 times lower than their reference values as indicated in Table 1 and the (estimated) free water diffusivities, respectively

Component	20% of D_{eff} 10^{-10} (m^2/s)	$Y_{CEX,7\text{-}ADCA}$ (-)	S/H (-)	D_{free} 10^{-10} (m^2/s)	$Y_{CEX,7\text{-}ADCA}$ (-)	S/H (-)
PGA	0.86	0.36	1.12	7.0[a]	0.42	1.20
7-ADCA	0.60	0.38	0.94	5.7[b]	0.41	1.25
CEX	0.50	0.35	0.81	4.3[c]	0.42	1.33
Reference		0.41	1.19		0.41	1.19

All simulations were done with 100 mM of the two substrates at 293 K and pH 8.0. The S/H was evaluated at the maximal CEX concentration (maximal conversion)
[a]Estimated equal to D_{free} of the similar component phenylacetate from Van der Wielen (1994)
[b]Estimated equal to D_{free} of the similar component 6-aminopenicillinate from Van der Wielen (1994)
[c]Adopted from Van der Wielen (1994)

The present model describes effects in terms of underlying fundamental processes. The fact that in this specific case the enzyme should be situated at the particle surface as much as possible may sound trivial, but is actually dictated by the diffusivities of the reactants. Because of the relatively low diffusivity of 7-ADCA in comparison with that of PGA, the internal concentration ratios of these substrates shift toward an unfavorably high PGA predominance, which is known to increase PGA hydrolysis and to reduce CEX synthesis (Schroën et al. 2002). Moreover, because the formed CEX is the slowest diffusing reactant, prolonged contact times with the enzyme increase secondary hydrolysis rates. However, in other bioconversions with other biocatalysts where multiple diffusion-limited reactions are in competition, other enzyme gradients (perhaps with an active core region) may be favorable. For such systems, the present modular physical model can easily be adapted for the specific geometry, kinetic parameters, flux equations, and mass balances at hand.

Besides enzyme loading, the intraparticle enzyme distribution and the particle radius, the ability of the reactants to diffuse through the particle also influences the particle performance. Understanding the precise mechanisms that determine the diffusivity of reactants into the matrix material is all but trivial, let alone the production of matrix structures with defined/designed resistances for mass transfer of specific reactants. Before even beginning to explore such possibilities in practice, it would be a good idea to establish the possible gain by model calculations. In this paragraph, the influence of (theoretical) alterations in reactant diffusivities was studied. For all reactants, one at a time, the reference diffusivity at 293 K (see Table 1) was increased or decreased by a factor 5, to evaluate the (predicted) effect on the CEX synthesis. Changes as a result of variation in diffusivities were found to be most noticeable for 7-ADCA, PGA, and CEX; therefore these are the only ones listed (Table 3).

Table 3 shows that when the diffusivity of 7-ADCA decreases, also the CEX yield and selectivity decrease. Low 7-ADCA diffusivities lead to low internal 7-ADCA/PGA ratios, which is known to reduce CEX formation and to increase PGA hydrolysis (Schroën et al. 2002). The opposite happens when the diffusivity of 7-ADCA was increased to its value in water.

When the PGA diffusivity was decreased, however, the yield and selectivity also decreased. In view of the line of reasoning just given for the 7-ADCA diffusivity, this was counterintuitive. Further investigation showed that the intraparticle PGA concentrations were reduced when the PGA diffusivity was lowered, as expected. At the same time, however, the pH gradients in the particle became very pronounced. Due to the absence of PGA (the main buffering component in the particle interior, p*K*a=7.2), the internal pH went up to 9.5 over a large portion of the particle interior. These high pH values are known to decrease CEX yield and selectivity (Schroën et al. 2002). On the contrary, when the PGA diffusivity was increased to the value in free water, the CEX yield and selectivity increased, and the pH remained below 8.4 within the entire particle.

Table 3 shows that a lowered CEX diffusivity has a strong negative impact on both the yield after CEX formation, which increases the risk of secondary hydrolysis. When the CEX diffusivity was increased, the opposite was observed, albeit that the effect is mainly on prevention of secondary hydrolysis (S/H increases, while the yield only increases slightly).

In retrospect, the model validation was successful: the course of the reaction of CEX synthesis experiments was predicted accurately for a broad range of substrate concentrations (between 50 and 600 mM and temperatures between 273 and 303 K). In contrast with our previous (purely macroscopic) model where mass transfer and enzyme kinetics were lumped into a set of fitted pseudokinetic constants (Schroën et al. 2002), the present physical model could also predict the course of the reaction at all pH values between 6 and 9, which ranges from almost free of diffusional limitation (pH 6) to severely diffusion limited (pH 9).

Apart from an accurate description of the macroscopic reaction, the model gave insight in the highly transient processes occurring within the particle. The model showed how diffusion limitation of substrates and products lead to suboptimal conversions in terms of yield and selectivity during the CEX synthesis. It further predicted the presence

of large intraparticle pH gradients, which were experimentally found and reported by Spieß and Kasche (2001).

Because the model gives an accurate description of the Assemblase-catalyzed CEX synthesis on the basis of physical and chemical phenomena that occur on a microscale inside the particle, it is very well-suited for the rational design of new biocatalysts for CEX production.

The modular design of the physical model facilitates its application in other systems. These may involve completely different reactions, catalyzed by other biocatalysts in other geometries. Ideally, the model will facilitate the process of biocatalyst production from a more or less trial and error approach to a truly rational design.

Acknowledgements Dr. Ruud van de Sman (Wageningen University) is kindly acknowledged for valuable discussions on process physics. Dr. Dimitris Stamatialis and Prof. Matthias Wessling from Twente University (The Netherlands) are acknowledged for fruitful discussions on mass transport of electrolytes. DSM and The Ministry of Economic Affairs of the Netherlands are kindly acknowledged for their financial support.

Appendix

The dissociation reactions that were considered are:

$$\begin{aligned} &CEX^0 \underset{}{\overset{r_{CEX}}{\rightleftharpoons}} CEX^- + H^+ \qquad PGA^+ \underset{}{\overset{r_{PGA}}{\rightleftharpoons}} PGA^0 + H^+ \\ &NH_4^+ \underset{}{\overset{r_{NH_3}}{\rightleftharpoons}} NH_3^0 + H^+ \qquad PG^0 \underset{}{\overset{r_{PG}}{\rightleftharpoons}} PG^- + H^+ \\ &OH^- + H^+ \underset{}{\overset{r_{water}}{\rightleftharpoons}} H_2O \end{aligned} \tag{22}$$

In addition, the following enzyme-catalyzed reactions were taken into account:

$$\begin{aligned} PGA^0 + 7\text{-}ADCA^- &\xrightarrow{R_{CEX,synth}} CEX^- + NH_3^0 \\ CEX^- &\xrightarrow{R_{CEX,hydro}} PG^0 + 7\text{-}ADCA^- \\ PGA^0 &\xrightarrow{R_{PG}} PG^0 + NH_3^0 \end{aligned} \tag{23}$$

with r_k the (fast) association/dissociation reaction rate of component k ($mol \cdot m^{-3} \cdot s^{-1}$), R_k the enzymatic reaction rate, which only takes place inside the biocatalytic particle ($mol \cdot m^{-3} \cdot s^{-1}$) The total cephalexin formation rate R_{CEX} is defined as the sum of the rates of CEX synthesis ($R_{CEX,synth}$) and CEX hydrolysis ($R_{CEX,hydro}$).

The following assumptions were made. The batch reactor is ideally and turbulently mixed, i.e., no concentration gradients of any component is present in the continuous bulk phase. The immobilization process of penicillin G acylase in Assemblase does not alter the intrinsic kinetics of the enzyme (Schroën et al. 2002). The polydisperse Assemblase particles can be represented by an equal volume of monodisperse spherical particles, which possess a single characteristic size, enzyme loading, and enzyme distribution. All resistance for mass transfer is located in the particle interior, i.e., no external diffusion limitations are present. Uniform mass transfer properties are assumed throughout the particle. This implicates that all transient processes, i.e., (electrostatic) diffusion and reaction, are radially symmetrical and can therefore be modeled in one dimension (along the radial axis). The flux of components inside the biocatalytic particles can be described with the Nernst–Planck flux equation for the ionic components (diluted solutions); for nonionic components, this reduces to the Fick flux equation.

As mentioned in the main text, the internal pH is altered by the enzymatic conversion (substrates and products have different pKa values). The arising mass and electrostatic gradients are a driving force for the fluxes of charged and uncharged components of which the fluxes of the ionic components are electrostatically coupled. The fluxes of all electrolytes, in turn, influence the local pH via local association/dissociation equilibria of all weak electrolytes. These rather complex interactions are incorporated in the proton balance. The balance for the continuous (water) phase is given (volume changes from titrant addition, no enzymatic conversion). Each M in Eqs. (24) and (25) refers to the mass balance as given in Eq. (8) in the main text into which the suitable flux equation (Eq. 9 for electrolytes) was substituted:

$$\left(\frac{dc_{H^+}}{dt}\right)_{ex} = \frac{\left[\begin{array}{l} M_{H^+} - M_{OH^-} - M_{PGA^0} - M_{NH_3} - M_{CEX^-} - M_{PG^-} \\ + \frac{1}{V_c}\frac{dV_c}{dt}\left(-c_{H^+} + c_{OH^-} + c_{PGA^0} + c_{NH_3} + c_{CEX^-} + c_{PG^-} + c_{titrant}\right) \\ + \frac{M_{PGA^+} + M_{PGA^0} - \frac{1}{V_c}\frac{dV_c}{dt}\left(c_{PGA^+} + c_{PGA^0}\right)}{1 + c_{H^+}/K_{PGA}} \\ + \frac{M_{NH_4^+} + M_{NH_3} - \frac{1}{V_c}\frac{dV_c}{dt}\left(c_{NH_4^+} + c_{NH_3}\right)}{1 + c_{H^+}/K_{NH_3}} \\ + \frac{M_{CEX^0} + M_{CEX^-} - \frac{1}{V_c}\frac{dV_c}{dt}\left(c_{CEX^0} + c_{CEX^-}\right)}{1 + c_{H^+}/K_{CEX}} \\ + \frac{M_{PG^0} + M_{PG^-} - \frac{1}{V_c}\frac{dV_c}{dt}\left(c_{PG^0} + c_{PG^-}\right)}{1 + c_{H^+}/K_{PG}} \end{array}\right]}{1 + \frac{K'_w}{c_{H^+}^2} + \frac{c_{PGA^0}}{K_{PGA} + c_{H^+}} + \frac{c_{NH_3}}{K_{NH_3} + c_{H^+}} + \frac{c_{CEX^-}}{K_{CEX} + c_{H^+}} + \frac{c_{PG^-}}{K_{PG^-} + c_{H^+}}} \tag{24}$$

with $K'_w = c_{H^+} c_{OH^-}$. With a constant pH in the continuous water phase, i.e., $\left(dc_H^+/dt\right)_{ex} = 0$, the volume change in time follows from Eq. (24):

$$\frac{dV_c}{dt} = V_c \frac{\left[-M_{H^+} + M_{OH^-} + M_{PGA^0} + M_{NH_3} + M_{CEX^-} + M_{PG^-} - \frac{M_{PGA^+} + M_{PGA^0}}{1 + c_{H^+}/K_{PGA}} - \frac{M_{NH_4^+} + M_{NH_3}}{1 + c_{H^+}/K_{NH_3}} - \frac{M_{CEX^0} + M_{CEX^-}}{1 + c_{H^+}/K_{CEX}} - \frac{M_{PG^0} + M_{PG^-}}{1 + c_{H^+}/K_{PG}}\right]}{\left[-c_{H^+} + c_{OH^-} + c_{PGA^0} + c_{NH_3} + c_{CEX^-} + c_{PG^-} + c_{titrant} - \frac{\left(c_{PGA^+} + c_{PGA^0}\right)}{1 + c_{H^+}/K_{PGA}} - \frac{\left(c_{NH_4^+} + c_{NH_3}\right)}{1 + c_{H^+}/K_{NH_3}} - \frac{\left(c_{CEX^0} + c_{CEX^-}\right)}{1 + c_{H^+}/K_{CEX}} - \frac{\left(c_{PG^0} + c_{PG^-}\right)}{1 + c_{H^+}/K_{PG}}\right]} \tag{25}$$

The external mass balance for PGA was given in the main text; the ones for the other (weak) electrolytes, CEX^-, NH_3 and PG^- are more straightforward:

$$\left(\frac{dc_{CEX^-}}{dt}\right)_{ex} = \frac{M_{CEX^0} + M_{CEX^-} - \frac{c_{CEX^-}}{K_{CEX}} \frac{dc_{H^+}}{dt} - \frac{1}{V_c} \frac{dV_c}{dt} \left(c_{CEX^0} + c_{CEX^-}\right)}{1 + c_{H^+}/K_{CEX}} \tag{26}$$

$$\left(\frac{dc_{NH_3^0}}{dt}\right)_{ex} = \frac{M_{NH_3^0} + M_{NH_4^+} - \frac{c_{NH_3^0}}{K_{NH_3^0}} \frac{dc_{H^+}}{dt} - \frac{1}{V_c} \frac{dV_c}{dt} \left(c_{NH_3^0} + c_{NH_4^+}\right)}{1 + c_{H^+}/K_{NH_3}} \tag{27}$$

$$\left(\frac{dc_{PG^-}}{dt}\right)_{ex} = \frac{M_{PG^-} + M_{PG^0} - \frac{c_{PG^-}}{K_{PG}} \frac{dc_{H^+}}{dt} - \frac{1}{V_c} \frac{dV_c}{dt} \left(c_{PG^-} + c_{PG^0}\right)}{1 + c_{H^+}/K_{PG}} \tag{28}$$

The conjugated counter forms of these biocatalytically active components were calculated from their respective equilibrium constants. For hydroxide ions, it follows from the water equilibrium that:

$$\left(\frac{dc_{OH^-}}{dt}\right)_{ex} = K'_w \frac{d\left(1/c_{H^+}\right)}{dt} = \frac{K'_w}{c_{H^+}^2} \frac{dc_{H^+}}{dt} \tag{29}$$

As a result of the addition of hydrochloric acid in the continuous (water) phase, the concentration of the inert chloride ions increases:

$$\left(\frac{dc_{Cl^-}}{dt}\right)_{ex} = M_{Cl^-} + R_{HCl} - \frac{c_{Cl^-}}{V_c} \frac{dV_c}{dt} \tag{30}$$

The rate at which HCl is added to keep the external pH at its set point is:

$$R_{HCl} = \frac{c_{HCl}}{V_c} \left(\frac{dV_c}{dt}\right)_{ex} \tag{31}$$

of which the last part was already declared in Eq. (25).

The internal mass balances are almost the same as the external ones. The differences are the presence of enzyme, i.e., enzymatic conversion terms (R_k), and the absence of

volume changes. As a final example, the internal mass balances for PGA and 7-ADCA are given:

$$\left(\frac{\mathrm{d}c_{\mathrm{PGA}^0}}{\mathrm{d}t}\right)_{\mathrm{in}} = M_{\mathrm{PGA}^0} + r_{\mathrm{PGA}} - R_{\mathrm{CEX}^-} - R_{\mathrm{PG}^0} \tag{32}$$

$$\left(\frac{\mathrm{d}c_{7-\mathrm{ADCA}^-}}{\mathrm{d}t}\right)_{\mathrm{in}} = M_{7-\mathrm{ADCA}^-} - R_{\mathrm{CEX}} \tag{33}$$

References

Bird RB, Stewart WE, Lightfoot EN (1960a) Transport phenomena. Wiley, New York, pp 495–518

Bird RB, Stewart WE, Lightfoot EN (1960b) Transport phenomena. Wiley, New York, pp 592–625

Cussler EL (2002) Diffusion: mass transfer in fluid systems, 2nd edn. Cambridge University Press, New York, pp 142–184

Do DD, Hossain MdM (1986) A novel method of determination of the internal enzyme distribution within porous solid supports and the deactivation rate constant. Biotechnol Bioeng 28:486–493

Duggleby HJ, Tolley SP, Hill CP, Dodson EJ, Dodson G, Moody PCE (1995) Penicillin acylase has a single-amino-acid catalytic centre. Nature 373:264–268

Hossain MdM, Do DD (1989) General theory of determining intraparticle active immobilized enzyme distribution and rate parameters. Biotechnol Bioeng 33:963–975

Perry R, Green DW (1997) Perry's chemical engineers handbook, 7th edn. McGraw-Hill, New York

Schroën CGPH, Nierstrasz VA, Moody HM, Hoogschagen MJ, Kroon PJ, Bosma R, Beeftink HH, Janssen AEM, Tramper J (2001) Modeling of the enzymatic kinetic synthesis of cephalexin—influence of substrate concentration and temperature. Biotechnol Bioeng 73:171–178

Schroën CGPH, Fretz CB, De Bruin VH, Berendsen W, Moody HM, Roos EC, Van Roon JL, Kroon PJ, Strubel M, Janssen AEM, Tramper J (2002) Modeling of the enzymatic kinetically controlled synthesis of cephalexin: influence of diffusion limitation. Biotechnol Bioeng 80:331–340

Spieß AC, Kasche V (2001) Direct measurement of pH profiles in immobilized enzyme carriers during kinetically controlled synthesis using CLSM. Biotechnol Prog 17:294–303

Svedas VK, Margolin AL, Berezin IV (1980) Enzymatic synthesis of β–lactam antibiotics: a thermodynamic background. Enzyme Microb Technol 2:138–144

Tramper J, Beeftink HH, Janssen AEM, Ooijkaas LP, Van Roon JL, Strubel M, Schroën CGPH (2001) Biocatalytic production of semisynthetic cephalosporins: process technology and integration. In: Bruggink A (ed) Synthesis of β-lactam antibiotics: chemistry, biocatalysis & process integration. Kluwer, Dordrecht, pp 206–249

Van der Wielen LAM (1994) Transients in the heterogeneous enzymatic deacylation of penicillin G. In: Van der Wielen LAM (eds) A countercurrent adsoprtive fluidized bed reactor for heterogeneous bioconversions. Ph.D. dissertation, Delft University of Technology

Van Roon JL (2005) Heterogeneity and scale in the rational design of an immobilized biocatalyst. Ph.D. thesis, Wageningen University

Van Roon JL, Joerink M, Rijkers M, Tramper J, Schroën CGPH, Beeftink HH (2003) Enzyme distribution derived from macroscopic particle behavior of an industrial immobilized penicillin G acylase. Biotechnol Prog 19:1510–1518

Van Roon JL, Groenendijk E, Kieft H, Schroën CGPH, Tramper J, Beeftink HH (2005a) Novel approach to quantify immobilized-enzyme distributions. Biotechnol Bioeng 89:660–669

Van Roon JL, Boom RM, Paasman M, Tramper J, Schroën CGPH, Beeftink HH (2005b) Enzyme distribution and matrix characteristics in biocatalytic particles. J Biotechnol 119(4):400–415 http://dx.doi.org/10.1016/j.jbiotec.2005.04.012

Van't Riet K, Tramper J (1991) Basic bioreactor design. Marcel Dekker, New York, pp 320–341

Weast RC, Astla MJ (1980) Handbook of chemistry and physics, 61st edn. CRC Press, Boca Raton